energies

MDPI

Article

Investigation of the Effect of Physical and Optical Factors on the Optical Performance of a Parabolic Trough Collector

Majedul Islam [1,3], Sarah Miller [2], Prasad Yarlagadda [1] and Azharul Karim [1,*]

1 Science and Engineering Faculty, Queensland University of Technology, Brisbane CBD, QLD 4001, Australia; murad99me@yahoo.com (M.I.); y.prasad@qut.edu.au (P.Y.)
2 Commonwealth Scientific and Industrial Research (CSIRO), 10 Murray Dwyer Circuit, Mayfield West, NSW 2304, Australia; sarah.miller@csiro.au
3 Department of Mechanical Engineering, Chittagong University of Engineering & Technology, Chittagong 4349, Bangladesh
* Correspondence: azharul.karim@qut.edu.au; Tel.: +61-7-31386879; Fax: +61-7-31381529

Received: 30 September 2017; Accepted: 2 November 2017; Published: 20 November 2017

Abstract: The overall thermal performance of a Parabolic Trough Collector (PTC) depends on its optical performance, particularly the uniformity of the irradiance distribution and the resultant optical efficiency of the collector. Local Concentration Ratio (LCR), optical efficiency and average light concentration are three fundamental parameters of the optical performance of a PTC. These parameters are affected by various optical and physical factors. The effects of these individual factors on the performance parameters were investigated in this study using a verified Monte Carlo ray tracing optical simulation model. The investigation revealed that all three performance parameters are directly related to the optical properties of the collector components. The values decreased gradually with the increase of focal length of the mirror. Uniformity of the LCR profile was observed to decrease with increasing rim angle and geometric concentration. Defocus dislocation of the receiver was found to improve the uniformity of the LCR distribution by decreasing its peak concentrations, C_{max}. Off-focus dislocation of the receiver, and inward angular deviation of the mirror profile were observed to increase the C_{max} and decrease the uniformity of the LCR distribition. Out-focus dislocation of the receiver and solar tracking error distort the bi-symmetry of a normal LCR profile.

Keywords: parabolic trough collector; concentrating solar power; optical efficiency; collector performance; uniformity of irradiance distribution

1. Introduction

Parabolic trough collectors (PCTs) usually comprise a parabolic reflector and a receiver through which a heat transfer fluid is circulated. The solar radiation reaching the PTC is reflected and focused onto the outer surface of a receiver absorber tube where the radiant energy is converted into thermal energy. This thermal energy is then conducted to the inner surface of the absorber tube and transferred to the heat transfer fluid by forced convection. This is considered a coupled heat transfer problem with complex geometrical conditions [1].

The PTC shown in Figure 1, consists of a single axis North-South tracking parabolic trough mirror that focuses solar radiation onto the receiver comprising an absorber tube surrounding by an evacuated glass envelope. Ideally, the receiver axis is coincident with the focal line of the mirror. The overall energy performance of the collector depends on its optical performance. The optical performance involves various parameters, including irradiance distribution around its receiver tube, optical efficiency (η_{opt}) and average light concentration (C_{avg}). These three performance parameters are affected by various

optical and physical factors including optical properties of the collector components, Direct Normal Irradiance (DNI), collector design parameters, and optical errors. Basic design parameters of the collector include its Geometric Concentration (GC), rim angle and the focal length of the mirror. The GC is the ratio of the mirror aperture area to the receiver surface area. For a given collector geometry, the irradiance distribution and the η_{opt} are significantly affected by its optical errors, including the receiver dislocation from the focus of the mirror, deviation of the mirror profile, and tracking error [2]. Optical optimization of the collector system from its design to operation requires explicit information to understand the contribution, or partial effects, of all these optical and physical factors on the performance parameters of the collector. However, the information leading to understanding is either not readily available or scarce in the open literature.

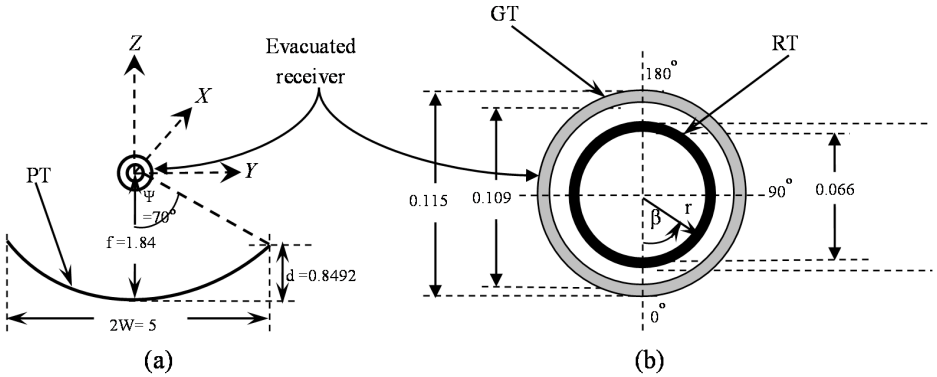

Figure 1. Cross-section of LS2 collector (all linear dimensions are in meter) and the coordinate system used in the ray tracing: (**a**) the Cartesian coordinate system, (X, Y, Z), for the complete collector, and (**b**) the Polar coordinate system, (X, r, β), for the tubular components such that $(X, Y, Z) = (X, \mathrm{r}\, sin\beta, -\mathrm{r}\, cos\beta)$ (in the figure, d, f, W and ψ are depth, focal length, half width and rim angle of the mirror, respectively, and the acronyms PT, GT and RT mean Parabolic Trough, Glass Tube and Receiver Tube, respectively).

The literature contains experimental investigations and theoretical studies performed to measure or predict the irradiance distribution along the perimeter of the tubular receiver of the collector preferably at ideal condition, and in some occasions, considering tracking error. The experimental investigations apply photogrammetry [3–5] and flux mapping [6,7], and theoretical studies apply cone optics [8–10] and Monte Carlo ray tracing [11–19]. Very few of these publications extensively addressed the effects of collector design and optical error parameters extensively on the optical performance parameters. Kalogirou et al. [20], and Thomas and Guven [2] investigated the effect of optical errors on both light interceptance and irradiance distribution of a PTC considering the total effect of all the errors as "effective sunshape", and the energy distribution was obtained applying a convolution technique. However, partial effects of different factors on the performance parameters are not evident from these studies.

This paper is part of a larger study, to design a hybrid photovoltaic-thermal collector that would provide uniform light distribution on the photovoltaic solar cells and improve the overall energy performance of the collector. A non-uniform flux on the PV solar cells could lead to considerable power loss from hot spots due to the Joule effect, resulting in an overall loss of PV efficiency [21,22]. The solar tracking error further increases the non-uniformity of the irradiance distribution. The voltage output of a concentrating PV solar cell increases logarithmically with irradiance intensity. The "shading effect", which is caused by non-uniformity of the irradiance on the PV aperture, reduces the overall electrical performance of the PV as the least irradiated cell limits the series current output. Therefore, it is critical to achieve uniform flux distribution in the aperture area of an integrated PV-thermal PTC.

Therefore, in this study, an extensive investigation was undertaken to explore the partial effects of various physical and optical factors on the optical performance of a standard PTC, and the information is made readily available to facilitate optical optimization of the collector in various phases

including design, fabrication, installation and operation. For this purpose, an MCRT simulation model was developed and validated. The MCRT model was implemented in a Zemax optical simulation packages [23]. To be able to verify the MCRT model directly, the Luz Solar 2 (LS2) [24] PTC used in the Solar Energy Generating Systems (SEGS) III-VII plants was modelled.

2. Method of MCRT Simulation

A cross sectional view of the 8 m long LS2 collector in a Cartesian coordinate system, and its evacuated glass enveloped receiver tube in a polar coordinate system are shown in Figure 1. A Cartesian coordinate system was used to calculate the instant spatial location and direction of movement of a ray. A cylindrical coordinate system was used to calculate the light incident location and intensity on the tubular components including the glass envelop and the receiver tube.

An ideal Parabolic Trough (PT) mirror was developed by adapting a bi-conic surface. The width, length and focal length of the mirror were 5 m, 7.8 m and 1.84 m respectively. On the other hand, the tubular components of the collector including the Receiver Tube (RT) and the Glass Tube (GT) were developed adapting two concentric annular volume objects. The inner diameters of the RT and the GT were 66 mm and 109 mm respectively, whereas the thicknesses of both tubes were 2 mm and 3 mm respectively. The receiver was larger than the mirror by 100 mm at both ends. An ideal coating system was enabled to get desired specular reflectance on the mirror, glass transmittance with anti-reflection coating and receiver absorptance with selective coatings.

Algorithm of the MCRT

Currently there is few systematic framework or modelling algorithm for MCRT available in the relevant literature. To overcome this gap, this study proposes a comprehensive framework to conduct MCRT simulation of parabolic trough concentrators. The algorithm developed is presented in Figure 2. The steps are easy to follow and are self-explanatory. The rhombuses represent arguments, while the rectangles are decisions of those arguments. All of these arguments and decisions are carried over by applying the fundamental theories and Monte Carlo (MC) concepts as discussed below. Detailed equations of the model can be found in the authors' previous publication [23]. The rays from the source to the receiver tube were traced according to the flow chart as illustrated in Figure 2. The statements inside the rhombuses are the MC statistical arguments, wile the answers of which depend on the sunshape, optical properties (mirror reflectance, glass transmittance and receiver absorptance), the geometry of the collector components, and the laws of reflection and refraction.

The rays were assumed to be emitted from a sunshape, $I(\varphi)$, as given by Equation (1) [25]. The azimuth angle and the deflection angle of the sunshape were 2π and 0.266°, respectively. The number of source rays per square meter of aperture area, N_{ray}, was chosen by considering errors in the mirror reflectance and the glass transmittance. The higher the number of rays, the lower the absolute error in the MCRT calculated value, as illustrated in Figure 3. Considering the computational time and efforts, 5×10^7 to 10×10^7 rays per square meter of aperture area of the sunshape were chosen for this MCRT model. Fresnel's law of reflection, Equation (2), describes the light reflected onto the mirror, and Snell's law of refraction, Equation (3), describes the light transmitted through the receiver glass tube.

$$I(\varphi) = \frac{Cos(0.05868\varphi/\pi)}{Cos(0.05544\varphi/\pi)} \tag{1}$$

where, φ is the deflection angle.

$$D_{PT} = D_n - 2(N_{PT} \cdot D_n)N_{PT} \tag{2}$$

$$D_{GT} = D_{PT} - (N_{GT} \cdot D_{PT})N_{GT} + \sqrt{(n_{GT})^2 - (n_{air})^2 + (N_{GT} \cdot D_{PT})^2 N_{GT}} \tag{3}$$

where, D_n, D_{PT} and D_{GT} are the directional vectors of the normal incident ray on the mirror aperture from the sun, reflected ray from the mirror and refracted ray through the glass tube respectively. Similarly, N_{PT} and N_{GT} are the normal vectors at the incident point of the rays on the mirror and the glass envelop respectively, while, n_{GT} and n_{air} are the refractive indices of the glass and air respectively.

The normal vectors N_{PT} and N_{GT}, are given by Equations (4) and (5) respectively.

$$N_{PT} = \frac{-P_{y\_PT}}{\sqrt{{P_{y\_PT}}^2 + 4f^2}} j + \frac{2f}{\sqrt{{P_{y\_PT}}^2 + 4f^2}} k \tag{4}$$

$$N_{GT} = \frac{P_{y\_GT}}{\sqrt{{P_{y\_GT}}^2 + {P_{z\_GT}}^2}} j + \frac{P_{z\_GT}}{\sqrt{{P_{y\_GT}}^2 + {P_{z\_GT}}^2}} k \tag{5}$$

where, P is the Cartesian coordinates of the incident points of the rays on the PT and the GT, and f is focal length of the mirror.

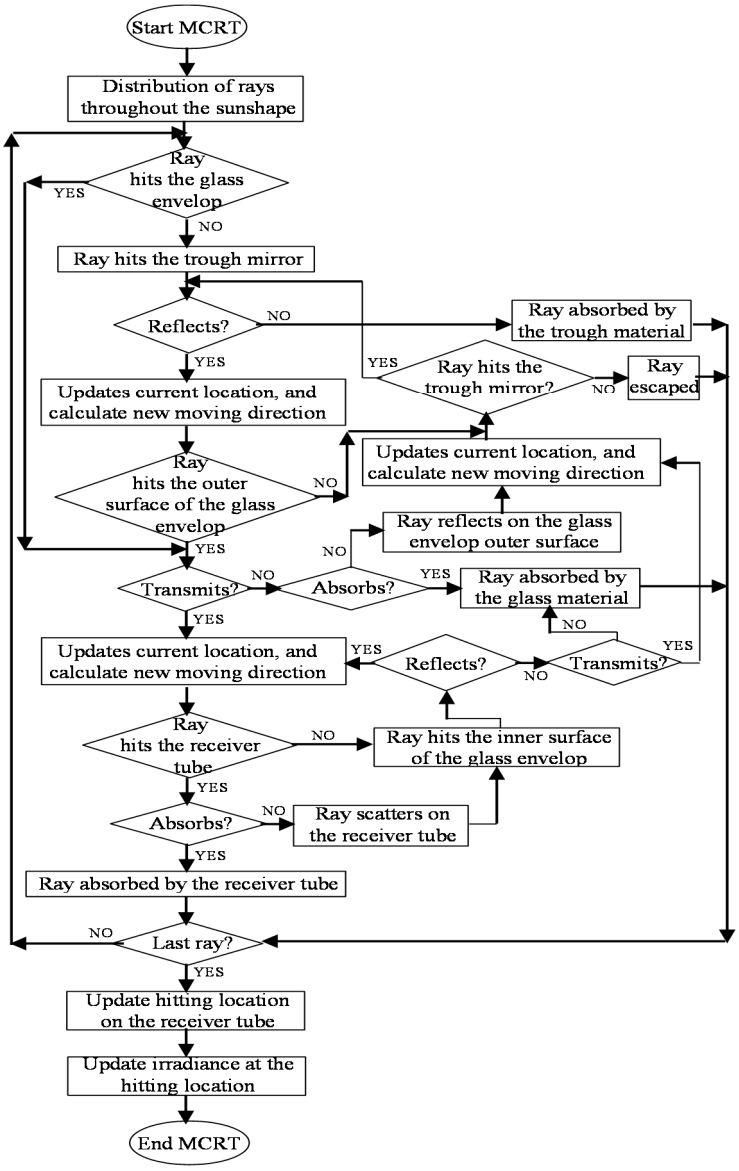

Figure 2. Framework for the Monte Carlo ray tracing model of Parabolic Trough Collector (PTC).

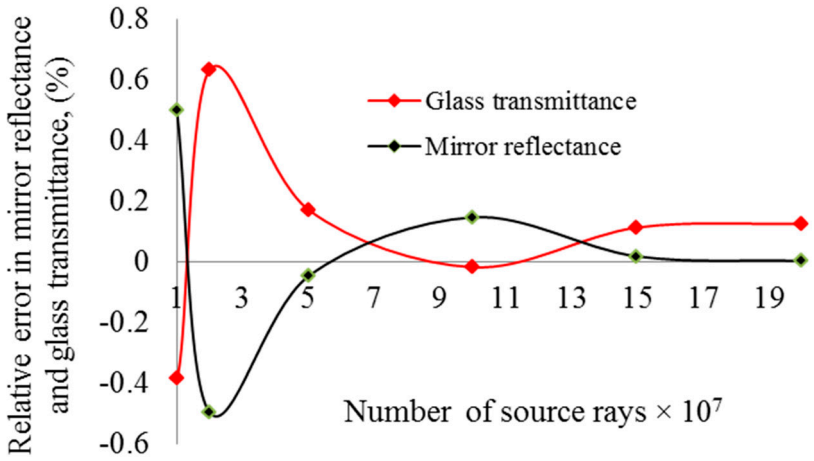

Figure 3. Optimum number of source rays per square meter aperture area, N_{ray}. Error = {(True value − MCRT calculated value) × 100%}/(True value). True value for mirror reflectance was 0.93 and for glass transmittance was 0.95.

3. Verification of the MCRT Model

Dudley et al. [24] measured the near optical efficiency, $(\eta_{opt})_{Expt}$, of the LS2 collector for two different selective coatings of the absorber tube, being cermet and black chrome, and three different conditions of glass envelop, being evacuated or vacuum, air filled and removed. The mirror was assumed to be perfect and have specular reflective, and the light incidence was assumed normal to the mirror aperture for simplification. Mirror reflectance (ϱ_{PT}), glass transmittance (τ_{GT}), and the absorptance of the cermet and the black chrome selective coatings were 0.9337, 0.935, 0.92 and 0.94 respectively [26]. Using the same test conditions as Dudley et al. [24], the optical efficiencies, $(\eta_{opt})_{MCRT}$, estimated using our MCRT model were compared with the experimental optical efficiencies, $(\eta_{opt})_{Expt}$, (see Table 1). The model slightly over estimated the efficiency; with the absolute deviations between 3.72% and 7.24% with an average of 6.19% which is reasonable given the simplifying assumptions.

Table 1. Selected test conditions of LS-2 collector from Dudley et al [24].

TC	DNI (W/m^2)	Selective Coatings	Glass Tube Condition	$(\eta_{opt})_{Expt}$ (%)	$(E_{est})_{Expt}$ (%)	$(\eta_{opt})_{MCRT}$ (%)	$(d_{abs})_{MCRT}$ (%)	$(d_{abs})_{avg}$ (%)
1	807.9	Cermet	Vacuum	72.63	1.91	77.89	7.24	6.19
2	925.1	Cermet	Air filled	73.68	1.96	76.42	3.72	
3	954.5	Cermet	Removed	77.5	-	82.59	6.57	
4	850.2	Black Chrome	Vacuum	73.1	2.36	78.38	7.22	

In the table, TC, DNI, η, E and d stand for Test Condition, Daily Normal Irradiance, Efficiency, Error and deviation. The suffixes opt, Expt, est, abs and avg mean optical, experimental, estimated, absolute and average.

Since, Dudley et al. [24] did not measure the irradiance distribution around the LS2 receiver, the irradiance profile calculated in this study was verified with Jeter's [8,9] analytical model. The GC, rim angle and the optical properties of the components of Jeter's collector were 20×, 90° and unity respectively. The DNI was 1 kW/m^2, which was incident normally on the collector aperture from a sunshape of 7.5 mrad angular radius. Jeter calculated the Local Concentration Ratio (LCR) around the receiver of an ideal collector such that LCR = I(β)/DNI. In this study, the LCR profiles of the collector with a 3.5 mm thick evacuated glass envelop around the absorber and without glass envelop were calculated, and compared against Jeter's analytical profile as shown in Figure 4. Both calculated profiles were found to be quite consistent with Jeter's analytical one. Jeter's analyses did not consider glass tube; which causes additional shading on the reflector (see the LCR at the 0° angular location of the receiver in the figure). The incoming rays striking the glass tube may be refracted towards

either the receiver tube or the mirror, altough with little chance to be reflected back to the receiver. The very good matching between current profiles and Jeter's profile confirms the reliability of the current MCRT model.

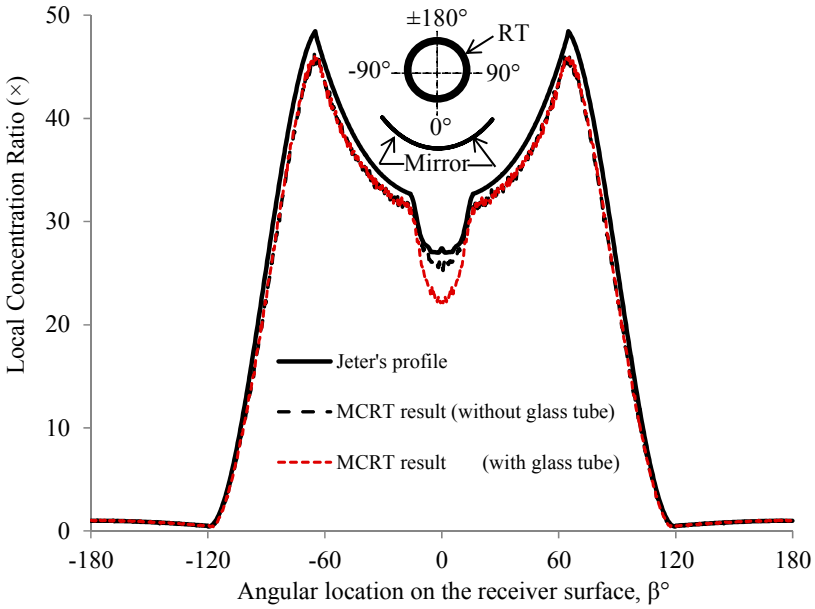

Figure 4. Comparison of calculated LCR profiles around the receiver tube (RT) of a typical PTC with Jeter's LCR profile.

4. Results of Parametric Analysis

The current MCRT model was employed to investigate partial effects of: (1) optical parameters, (2) design parameters, and (3) optical error parameters on the LCR distribution around the receiver tube, η_{opt}, and C_{avg} of the collector. The η_{opt} and C_{avg} were normalised by dividing a certain value by their respective maxumum value for a certain analysis. Where deemed reasonable, the uniformity of the LCR distribution was analyzed quantitatively by quantifying as minimum light concentration (C_{min}), maximum light concentration (C_{max}), average light concentration (C_{avg}), and Mean Absolute Deviation (MAD). The C_{min}, C_{max} and C_{avg} were estimated along the periphery of the cross-section of the absorber tube. The MAD was calculated as average of the absolute deviations of LCRs from their respective C_{avg}. The rim angle and the focal length of the mirror were about 70° and 1.84 m respectively, and the GC of the collector was around 22.74×. The DNI was assumed as 1 kW/m^2. Local specular reflectance of the mirror and the absorptance of the bare receiver were assumed 0.9335 and unity respectively.

The characteristics of the LCR profiles were analysed against a normal LCR profile under ideal conditions as calculated using the current MCRT model and shown in Figure 5. The normal profile was found to be bi-symmetric about 0°–180° axis of the receiver, and almost uniform along the length of the receiver. A normal LCR profile of a PTC under ideal conditions was found to contain four distinct zones, termed as: A: Receiver Shadowing (RS) zone, B: Concentration Increasing (CI) zone, C: Concentration Falling (CF) zone, and D: Direct Sun (DS) zone. RS is the shadowing effect of the receiver on the mirror, which impact the area upto about 15° in the LS2 receiver. Inclusion of the glass envelope was observed to increase the shadowing effect (see Figure 4). Once the shadowing effect is diminished, the rest of the light concentrates on the receiver within around 45° angular location and raise the C_{max} exponentially that forms the CI zone. As soon as the CI zone has peaked to C_{max}, the concentration falls rapidly within 90° angular location of the receiver, which is called CF zone; and no more concentrated light is available. However, the upper half of the receiver receives the light from direct sun, which is called DS zone. Investigation revealed that this normal LCR profile is affected

significantly by collector design variations and optical errors. It was also observed that η_{opt}, and C_{avg} were affected also by the optical properties of the collector components as explained below.

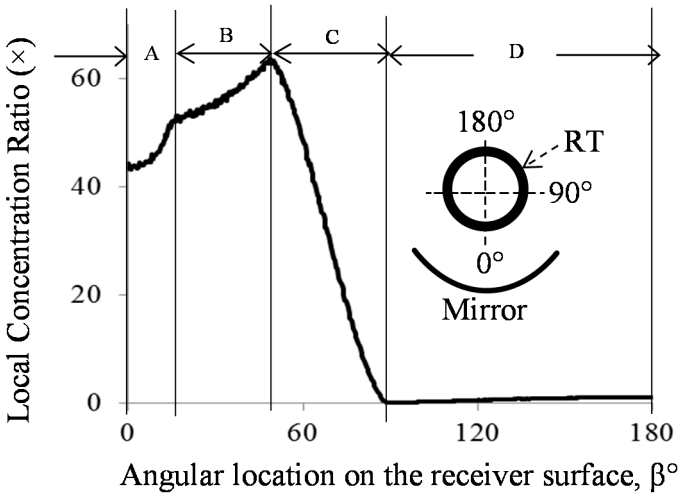

Figure 5. LCR profile around the receiver tube (RT) of the LS2 collector at ideal condition. The profile is bi-symmetric about 0°–180° axis of the receiver, and theoretically uniform along the length of the receiver. The LCR profile contains four distinct zones, such as, **A**: Receiver Shadowing (RS) zone; **B**: Concentration Increasing (CI) zone; **C**: Concentration Falling (CF) zone, and **D**: Direct Sun (DS) zone.

4.1. Effect of Optical Properties of the Collector, DNI and Glass Envelop Thickness

The optical properties of the collector includes the mirror reflectance, glass transmittance and receiver absorptance. The effect of these properties; the DNI, and the thickness of the glass envelope; on the optical performance of a PTC were investigated as presented in Figure 6.

As the figure shows, the LCR, C_{avg} and η_{opt} were observed to be directly proportional to the mirror reflectance, glass transmittance. The DNI was also observed to have a directly proportional impact on LCR and C_{avg}, and, however, very little indirect effect on η_{opt}. The glass envelop thickness was found to have very little and indirect impact on the optical performance parameters. None of these factors was found to modify the normal shape but vary the local value of the LCR profile.

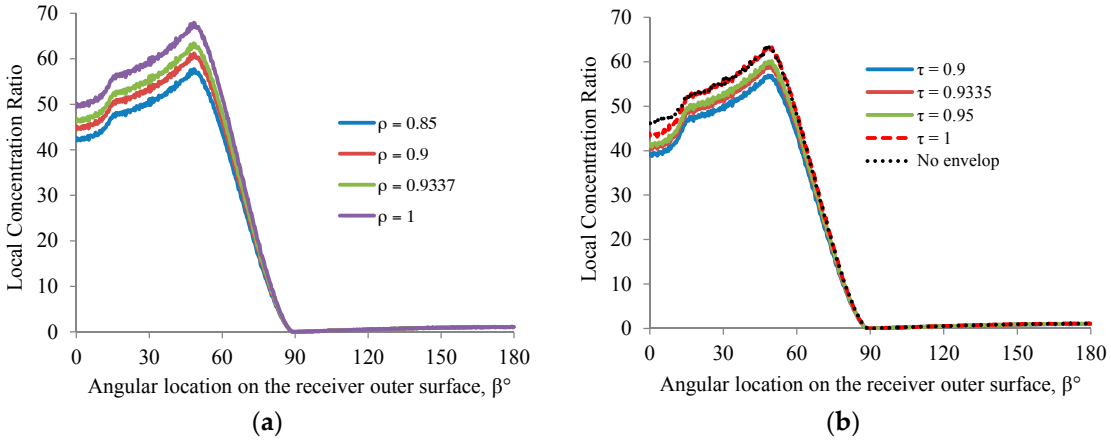

Figure 6. *Cont.*

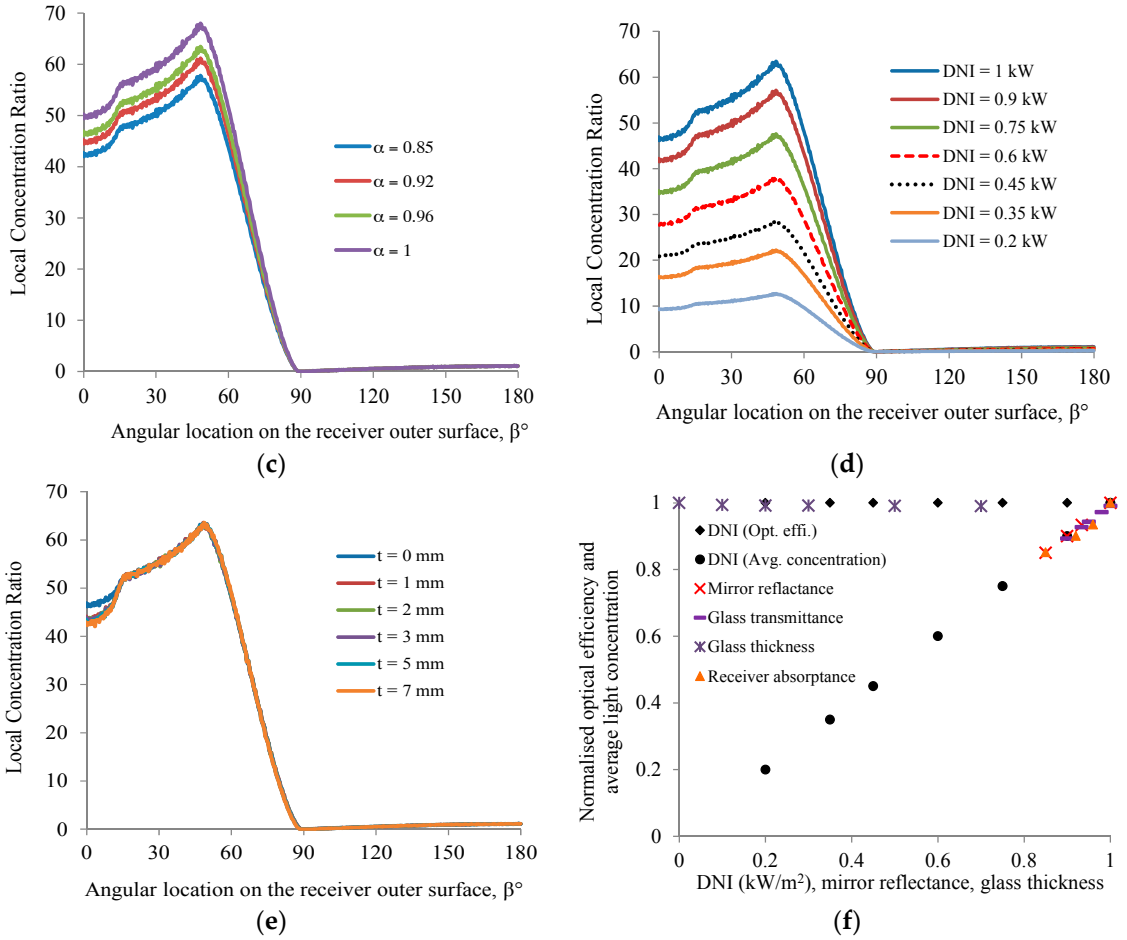

Figure 6. Effect of (**a**) mirror reflectance; (**b**) glass transmittance; (**c**) receiver absorptance; (**d**) DNI and (**e**) glass thickness on the LCR distribution around the receiver tube, and (**f**) effect of these parameters on the normalised optical efficiency, η_{opt}, and normalised average light concentration, C_{avg}, of the collector. (These values were normalised dividing by their respective maxumum value).

4.2. Effect of Design Parameters of the Collector

Focal length, rim angle and GC are three fundamental design parameters of a PTC. Focal length is the characteristic parameter of a parabolic mirror. The depth and width of the mirror depend directly on the rim angle. On the other hand, GC is the ratio of the mirror aperture area to the receiver surface area. The GC of a PTC can be varied either by varying the receiver diameter or mirror width independently or both together. However, variation of the mirror width causes variation of the rim angle. The effects of rim angle and GC on the optical performance of a PTC were investigated with a mirror of fixed focal length, and with mirrors of different focal lengths as described below.

4.2.1. Effect of Rim Angle and GC with a Mirror of Fixed Focal Length

The GC was increased by decreasing the receiver diameter for a fixed rim angle. In addition, the rim angle was increased by increasing the trough width for a fixed receiver diameter, which is also increased the GC. The effects of these parameters on the optical performance parameters were analysed as presented in Figures 7 and 8 and Table 2.

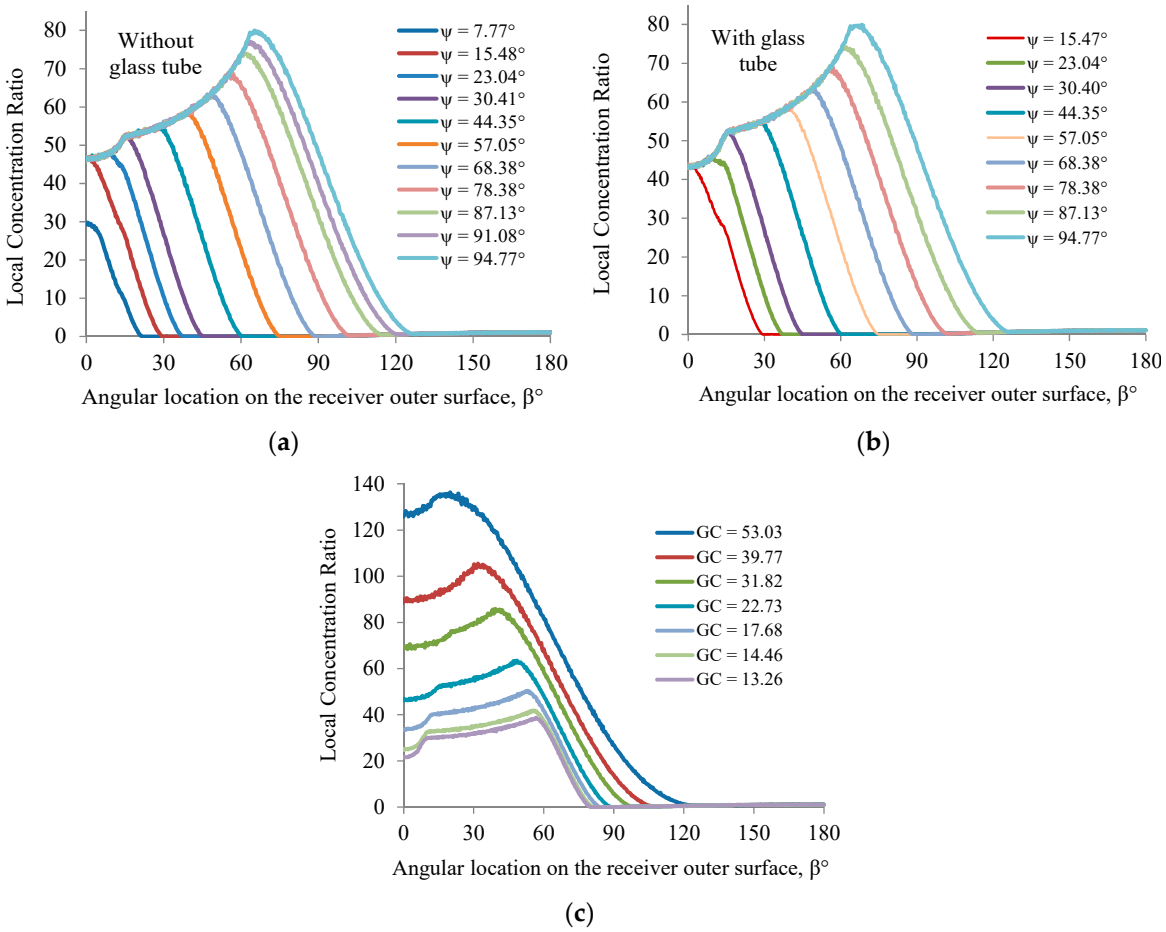

Figure 7. Effect of rim angle for, (**a**) the receiver without glass envelop and (**b**) the receiver with glass envelop, and (**c**) the effect of Geometric Concentration (GC) on LCR profile of a PTC with a mirror of fixed focal length.

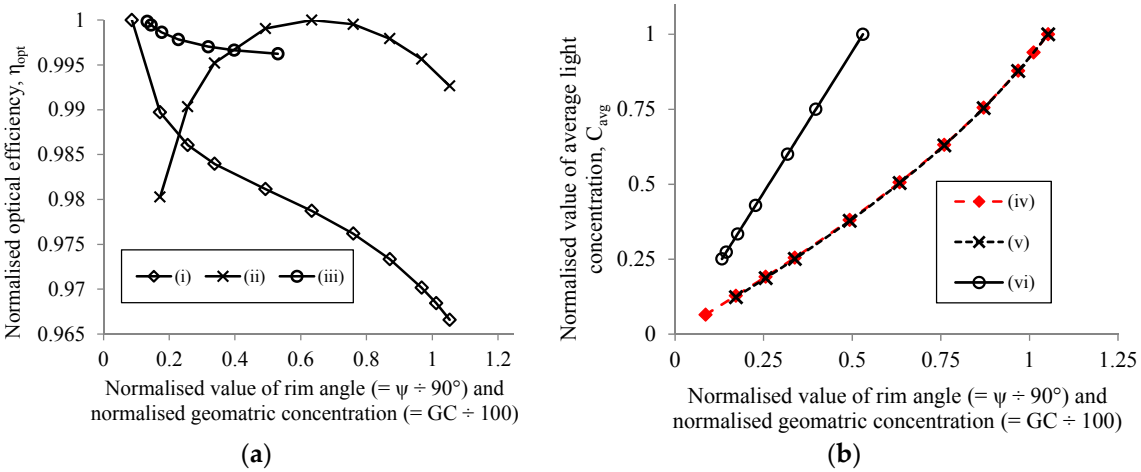

Figure 8. (**a**) Effect of, (**i**) rim angle for the receiver without glass envelop; (**ii**) rim angle for the receiver with glass envelop and (**iii**) GC on normalised η_{opt} of a PTC; and (**b**) effect of, (**iv**) rim angle for the receiver without glass envelop; (**v**) rim angle for the receiver with glass envelop and (**vi**) GC on normalised C_{avg} of a PTC.

Table 2. Effect of design parameters on the uniformity of the LCR distribution around the receiver of a PTC.

Variation of Mirror with Different Focal Length			C_{min} (sun)	C_{max} (sun)	C_{avg} (sun)	MAD
Ideal LS2 collector, GC = 22.74, ψ ≈ 70°, f = 1.84 m			0	63.5	21.8	23.7
Mirror focal length is fixed	d_o = V ψ = C	GC = 53.03	0.5	136.8	50.9	48.7
		GC = 13.26	0	38.7	12.8	14.2
	d_o = C W = V	ψ = 44.35°	0	55.3	13.2	17.6
		ψ = 87.13°	0.4	74.3	30.4	26.3
Mirror focal length is variable	GC = C ψ = V	f = 1.4 m	0.2	57.4	22.0	20.5
		f = 3 m	0	85.0	21.4	27.2
	GC = V ψ = C	f = 1.4 m	0	50.4	16.8	18.5
		f = 3 m	0.2	96.0	34.6	35.5
	GC = C ψ = C	f = 1.4 m	0	64.4	22.1	23.9
		f = 3 m	0	61.2	20.9	22.8

In the table: LS2 = Luz Solar 2 collector, sun = unit of light concentration = 1 kW/m^2; C_{min}, C_{max} and C_{avg}, and MAD stand for minimum, maximum and average light concentration, and Mean Absolute Deviation; GC = Geometric Concentration, ψ = rim angle, f = focal length, d_o = outer diameter of the receiver, W = half width of the mirror, V = variable and C = constant or fixed.

Figure 7a,b show that increasing the rim angle extends the Concentration Increasing zone by increasing the C_{max}. Therefore, the light coverage at the bottom of the receiver was found to be increasing, and the Direct Sun region was decreasing with rim angle. Moreover, as the C_{max} was estimated to be increasing, the Concentration Falling zone was also extending with rim angle. However, the slope of the CI zone was found to be independent of the rim angle and they were found to be almost parallel with each other at all rim angles. The presence of the glass envelop was observed to increase shadowing on the mirror, as a result, the Receiver Shadowing zone became deeper.

As shown in Figure 8a,b, the η_{opt} was decreasing gradually and the C_{avg} was increasing exponentially with increasing of rim angle. The η_{opt} of the receiver without the glass envelop was predicted to drop by around 4% in total until a 90° rim angle. On the other hand, the η_{opt} was estimated to be increased by about 2% in total until a 70° rim angle and then decreased by about 0.5% until a 90° rim angle. However, the graphs of the C_{avg} for both the conditions: with and without glass envelop, were found almost superimposed to one another (see Figure 8b).

When the GC was increased by decreasing the receiver diameter, the same amount of light was concentrating on a smaller surface area of the receiver. Therefore, although C_{max} was increasing, the Concentration Increasing zone was not extending; rather this zone was merging with Receiver Shadowing zone (see Figure 7c). The slope of the Concentration Falling zone was observed to be decreasing gradually with increasing GC. Since, the mirror width was not increasing, the increase of GC had an indirect, but, insignificant effect on the η_{opt}, as can be seen from Figure 8a. However, as the receiver surface area was decreasing with the increase of GC, the C_{avg} was observed to be increasing linearly (see Figure 8b).

As presented in Table 2, the increase of both rim angle and GC for fixed focal length were observed to increase non-uniformity of the LCR dsitribution. The non-uniformity was observed more sensitive to the GC than the rim angle. For instance, the MAD was estimated to be increased rapidly from 14 to 49 for the GCs between 13 and 53, whereas, that was estimated to be increased from 18 to 26 for the rim angles between 44° and 87°.

4.2.2. Effect of Mirrors of Different Focal Lengths

Focal length is a characteristic parameter of a parabolic mirror. A variation of focal length refers to a variation of the mirror with a certain focal length. The effects of varying the focal length on the

optical performance parameters were investigated for various rim angles and GCs. The effects are shown in Table 2, Figures 9 and 10.

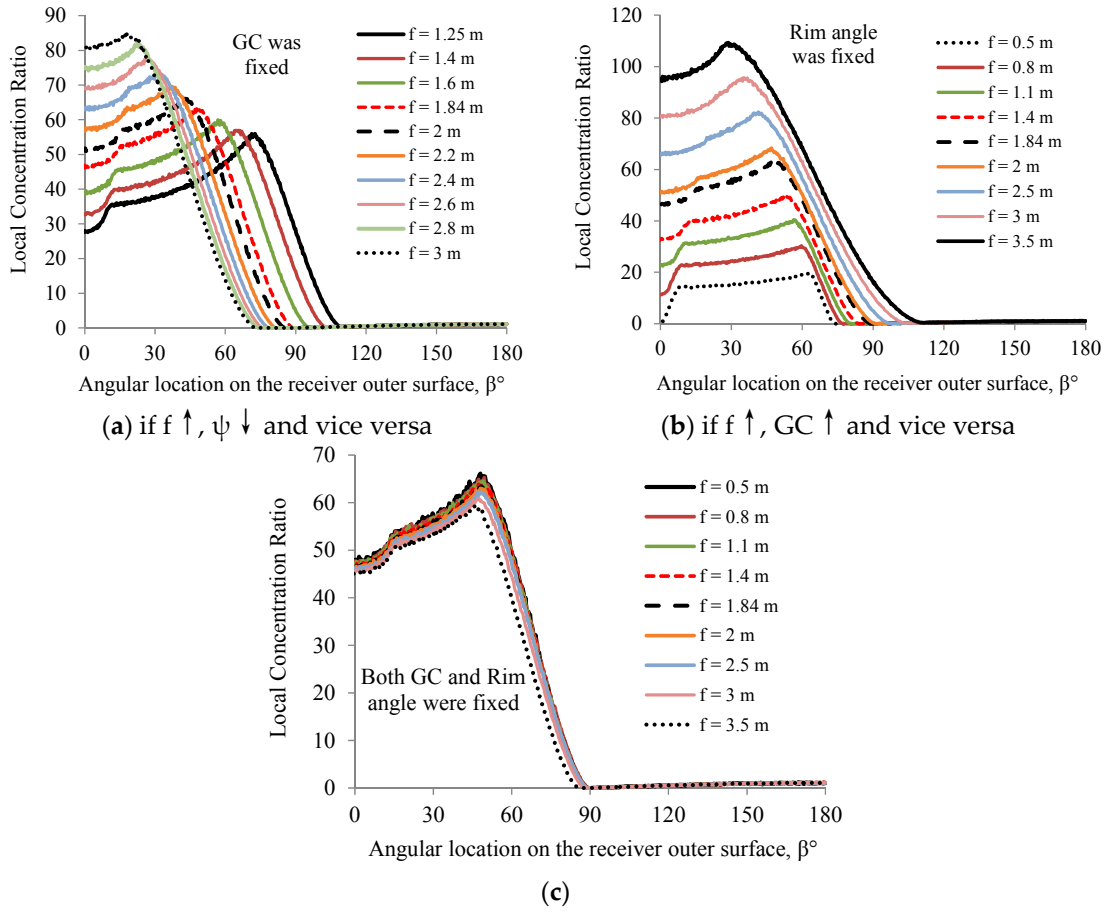

Figure 9. Effect of mirror variations in terms of their focal length, f, on local oncentration ratio profile of a PTC for: (**a**) Fixed Geometric Concentration (GC). The receiver outer diameter and the mirror aperture width are fixed. So a mirror of a larger focal length has a smaller rim angle and vice; (**b**) Fixed rim angle, ψ. As the receiver outer diameter and rim angle are fixed, a mirror of a larger focal length has an larger aperture width, and so a larger GC, and (**c**) fixed GC and rim angle.

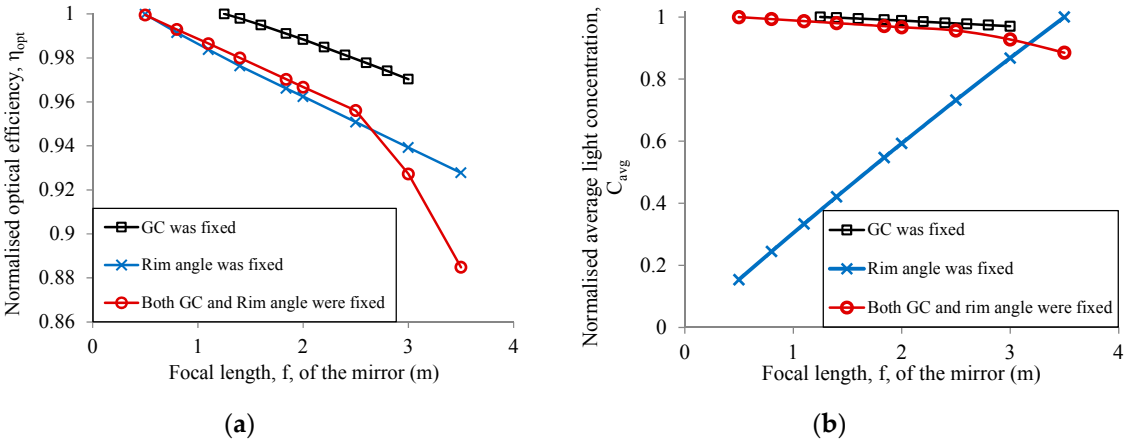

Figure 10. Effect of mirror focal length on (**a**) normalised η_{opt} and (**b**) normalised C_{avg} for different rim angle and GC.

For a PTC with fixed GC for a fixed receiver, the mirror of a larger focal length has smaller rim angle. So, the light is concentrated onto a smaller surface area of the receiver, and the C_{max} was increasing gradually with the increase of focal length as shown in Figure 9a. As a result, the Receiver Shadowing zone and the Concentration Increasing zone were observed to be gradually merging with each other with increasing focal length. Thus, C_{max} was estimated to increase from around 55 suns to 85 suns with an increase in mirror focal length from 1.25 m to 3 m. The Concentration Falling zones of all LCR profiles were found almost parallel to each for all focal lengths as shown in the same figure. The increase of focal length was observed to have adverse effect on the η_{opt} and C_{avg}. Both the performance parameters were estimated to be dropped almost linearly by around 3% for the focal length variation between 1.25 m and 3 m as is shown in Figure 10.

On the other hand, for a PTC with fixed rim angle and fixed receiver diameter, the larger the focal length of the mirror, the larger the GC of the collector and vice versa. Therefore, C_{max} was observed to be increasing, the Receiver Shadowing and Concentration Increasing zones merging together, the slope of the Concentration Falling zone was decreasing, and the Direct Sun zone was shortening gradually with the increase of focal length as shown in Figure 9b. However, while C_{avg} was observed to be increasing, η_{opt} was decreasing linearly with increasing focal length as illustrated in Figure 10. The calculated η_{opt} was dropped by about 6% as the focal length increased from 0.5 m to 3.5 m.

Finally, the sole effect of mirror focal length on the optical performance of a PTC was investigated for a fixed rim angle and fixed GC. The magnitudes of the LCR were estimated to be gradually decreasing with increasing focal length, although the LCR profiles were almost parallel to each other (see Figure 9c). Both η_{opt} and C_{avg}, were found to drop by about 12% as the focal length increased from 0.5 m to 3.5 m. In addition, the drop also gradually increased with increasing focal length.

As presented in Table 2, when the GC was varied, GC =V in the table, the uniformity of the LCR profile was found to decrease more quickly than that when the rim angle was varied with an increase in focal length. The MAD estimated was almost doubled for the variable GC case, while MAD increased by only one third for the variable rim angle case with an increase of focal length from 1.4 m to 3 m. However, MAD was found to decrease slightly from 24 to 23 when the range of focal lengths was varied under fixed rim angle and GC conditions.

4.3. Effect of Optical Errors

Optical errors including dislocation of the receiver from the focus of the mirror, deviation of the mirror profile from its ideal parabolic shape, and tracking error can affect the optical performance of the collector adversely. The partial effect of all these individual errors on the optical performance parameters of the collector were investigated as described below.

4.3.1. Effect of Dislocation of the Receiver

A faulty assembly or structural deformation may cause dislocation of the receiver from the focus of the mirror. The dislocation can modify the LCR, and may have an adverse impact on the optical performance of a collector. Referring to Figure 11, the dislocation was assumed along three different directions: off-focus (↑ in the figure), defocus (↓ in the figure) and out-focus (→ in the figure). The dislocation, d, was expressed as dimensionless value dividing by the radius, r, of the receiver. The findings are described in Figure 11 and Table 3.

The light was observed to be gradually concentrating on smaller surface area at the bottom (at $\beta = 0^{\circ}$) of the receiver with an increase in off-focus dislocation as illustrated in Figure 11a. The LCR profile was becoming Gaussian in shape diminishing the Receiver Shadowing and Concentration Increasing zones completely into the Concentration Falling zone. As a result, C_{max} reached 240 suns at a unit off-focus dislocation ($d\uparrow = r$). The CF zone was moving towards the RS zone, and the Direct Sun zone was extending with the gradual increase of dislocation. The off-focus dislocation was found increase the non-uniformity of the LCR profile gradually. From Table 3, it can be seen that the MAD was increased from 23.7 to 33 when the receiver was dislocated by 77% of its radius.

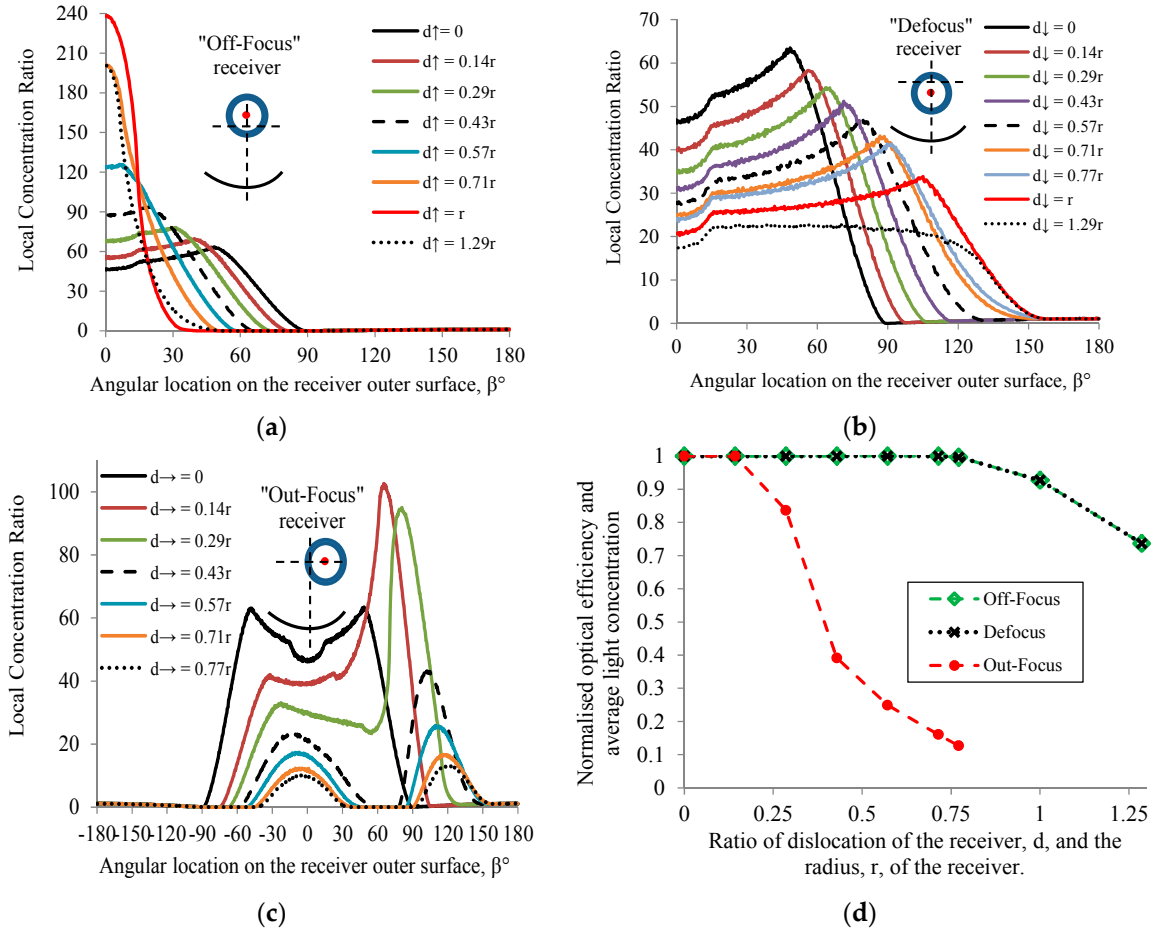

Figure 11. Effect of receiver dislocation on the LCR profile of the receiver: (**a**) off-focus; (**b**) defocus and (**c**) out-focus, and (**d**) on the η_{opt} and C_{avg} of the collector. (Here, 'r' is the radius of the receiver, 'd' is the amount of dislocation, and the arrows show the direction of dislocation).

Table 3. Effect of collector operating conditions on the uniformity of the LCR distribution around the receiver of a PTC.

Error of the Collector Elements			C_{min} (sun)	C_{max} (sun)	C_{avg} (sun)	MAD
Ideal LS2 collector, GC = 22.74, ψ ≈ 70°, f = 1.84 m			0	63.5	21.8	23.7
Receiver dislocation	Off-focus	d↑ = 0.14r	0.0	69.6	21.8	25.5
		d↑ = 0.77r	0	216.4	21.7	33.2
	Defocus	d↓ = 0.14r	0.116	58.9	21.9	21.9
		d↓ = 0.77r	1.0	41.6	21.8	12.4
	Out-focus	d↔ = 0.14r	0.0	102.6	21.8	23.4
		d↔ = 0.77r	0	13.4	2.8	3.2
Tracking error		0.2°	0	69.7	21.7	23.4
		1°	0.0	35.9	9.0	10.8
Mirror profile deviation	Inward deviation	Û = 0.05°	0	71.0	21.8	24.8
		Û = 0.375°	0	109.8	21.8	30.0
	Outward deviation	Ŭ = 0.05°	0.062	64.0	21.9	22.5
		Ŭ = 0.35°	0	67.0	21.9	21.9

In the table: LS2 = Luz Solar 2, sun = unit of light concentration = 1 kW/m^2; C_{min}, C_{max} and C_{avg}, and MAD stand for minimum, maximum and average light concentration, and Mean Absolute Deviation; GC = Geometric Concentration, ψ = rim angle, f = focus, d = amount of dislocation, r = radius of the receiver and the arrows show the directions of dislocation of the receiver from the focus of the mirror.

On the other hand, the effect of defocus dislocation of the receiver on the LCR distribution and its uniformity observed was almost the reverse to that of the off-focus dislocation. As shown in Figure 11b, the concentrated light was observed to be gradually occupying more surface area at the bottom (at $\beta = 0°$) of the receiver, which was flattening the Concentration Increasing zone, and shrinking the Direct Sun zone gradually. As a result, C_{max} was dropped to 30 suns at unit defocus dislocation ($d\downarrow = r$). This dislocation was observed to increase the uniformity of the LCR profile. The MAD was dropped to 12 from 33 for 0.77r defocus dislocation (see Table 3).

Both these dislocations were found to have equal and very little effect on the η_{opt} and the C_{avg} till 0.75r ($d\updownarrow = 0.75$) dislocation as shown in Figure 11d. Dislocation of more than 0.75r was found to affect η_{opt} and C_{avg} adversely as the light was missing the receiver.

On the other hand, out-focus dislocation of the receiver was observed to diminish the normal bi-symmetry of the LCR profile as shown in Figure 11c. The η_{opt} and C_{avg} were observed to be decreased rapidly after just 0.14r out-focus dislocation ($d\leftrightarrow = 0.14r$) as shown in Figure 11d. Table 3 shows that, the C_{max} and the C_{avg} were dropped from 103 suns to 13 suns at 0.14r dislocation and 22 suns to 3 suns at 0.77r dislocation, respectively.

4.3.2. Effect of Deviation of Parabolic Profile of the Mirror

Perfection of the parabolic profile of a PTC mirror is one of the most important prerequisites for its standard optical performance. Since, any external load such as wind load or dead load during operation may distort a mirror from its ideal profile; one way to simulate this is through rotation of the mirror halves around its vertex. The actual aperture width will decrease for inward ($\hat{U}°$) rotation and will increase for outward ($\check{U}°$) rotation from the ideal as shown in Figure 12. The effects of these deviations on the optical performance of the PTC were investigated as illustrated in Figure 13.

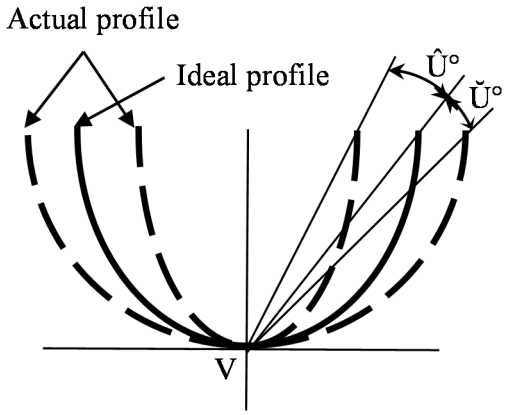

Figure 12. Actual profile versus ideal profile of a parabolic mirror. In the figure, V is the vertex of the parabola, and $\hat{U}°$ and $\check{U}°$ are the inward and outward angular rotation of two halves of the mirror with respect to the vertex from its ideal profile respectively.

From Figure 13a, the concentrated light was observed to occupy a gradually smaller surface area at the bottom of the receiver with an increase of inward angular deviation of the mirror profile. This deviation was found to reverse the slopes of the Receiver Shadowing and Concentration Increasing zones gradually one after another. Eventually, these RS and CI zones aligned with the Concentration Falling zone, and formed a Gaussian LCR profile with the increase of the deviation. The highest value of C_{max} was estimated to be around 110 suns at 0.375° inward deviation. On the other hand, from Figure 13b, outward deviation ($\check{U}°$) of the mirror was observed to increase the shadowing effect at the bottom of the receiver; and eventually a complete shadow was observed at 0.15° deviation. The shadow was found to further increase towards ±90° angular location of the receiver with increasing deviation.

As shown in Figure 13c, the effect of the deviation (both inward and outward) on η_{opt} and C_{avg} were found to be almost equal and similar. The η_{opt} and C_{avg} were estimated to be decreased slightly till 0.375° angular deviation and then decreased rapidly. As Table 3 shows, the inward deviation was observed to increase the non-uniformity of the LCR distribution, whereas, the outward deviation was observed to have little effect on the uniformity of the LCR profile. The MAD was estimated to be increased by 6 points for 0.375° deviation from the ideal profile, whereas the same was decreased by almost 2 points 0.35° outward deviation.

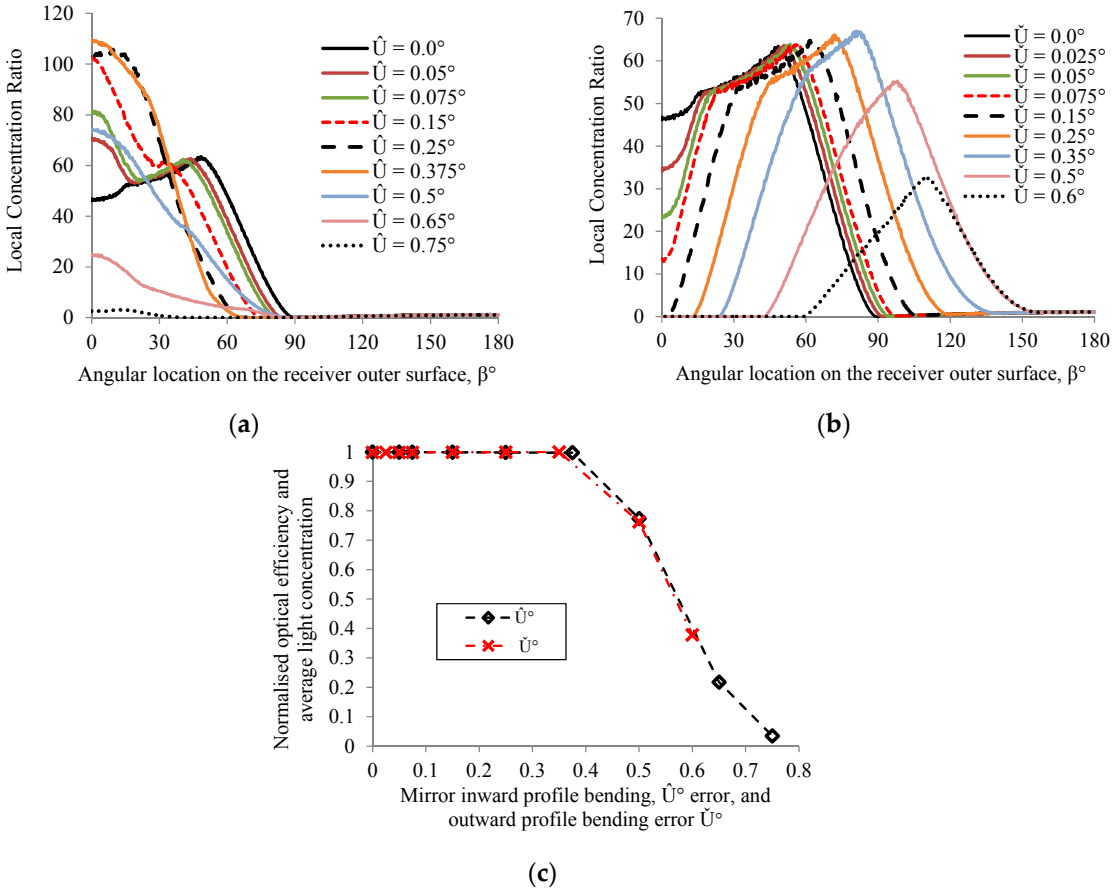

Figure 13. Effect of (**a**) inward deviation and (**b**) outward deviation of the mirror profile on the LCR profile of the receiver, and (**c**) on the η_{opt} and C_{avg} of the collector.

4.3.3. Effect of Tracking Error

A (single axis) solar tracking system is used for the PTC system to track the sun and maintain it (the sun) at the sagittal plane of the collector. Any angular deviation between the incident light and the plane of symmetry of the mirror called the sun tracking error could affect the optical performance of the collector significantly. The effect of the sun tracking error, $E_{Tracking}$, was investigated, and the result is presented in Figure 14 and Table 3.

As shown in Figure 14a, similar to the case of out-focus dislocation of the receiver, tracking error was observed to distort the bi-symmetry of normal LCR profile. As a result, a single peak concentration in the receiver LCR profile was seen at the side of tracking error; and the magnitude of the peak was calculated to be gradually increasing with the tracking error until around $E_{Tracking}$ = 0.6°. The Receiver Shadowing and the Concentration Increasing zones of the LCR profile at the opposite side of the tracking error were found to be diminishing in the Concentration Falling zone gradually with the increase of the error. The η_{opt} and C_{avg} were estimated to be decreasing very slowly till around 0.6° tracking error, and then decreasing fairly quickly afterwards (see Figure 14b). In Table 3, the MAD was

calculated to drop from 23.7 to 10.8 for $E_{Tracking}$ = 1.0°. However, C_{max} and C_{avg} were also calculated to drop proportionately from 63.5 to 36 and from 22 to 9 respectively at that tracking error.

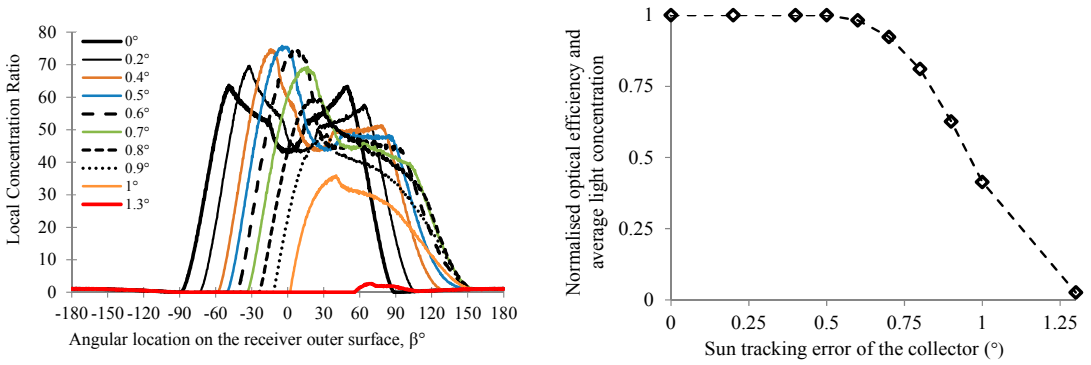

(**a**) (**b**)

Figure 14. Effect of tracking error (°) on (**a**) LCR profile of the receiver and (**b**) on the η_{opt} and C_{avg} of the collector.

5. Conclusions

The effect of optical parameters, design parameters, and optical errors on the LCR distribution, η_{opt} and C_{avg} is comprehensively investigated. The optical properties of the collector components were found to be directly proportional to the LCR, η_{opt} and C_{avg}. The DNI also showed a directly proportional effect on the LCR and C_{avg}. However, DNI had no significant effect on the η_{opt} of the collector.

An increase in GC and rim angle was observed to increase the non-uniformity of the LCR distribution around the receiver of a PTC. However, the uniformity was observed to be affected more by GC than the rim angle. Larger rim angles were found to concentrate more light. Therefore, optimally a smaller GC and larger rim angle are recommended to achieve relatively more uniform light distribution around the receiver, and more energy output.

A glass envelop around the receiver was observed to improve the optical efficiency of a PTC collector. The η_{opt}, which was predicted to be dropped by about 4% in 90° rim angle for a bare receiver, was increased by about 2% in 70° rim angle before dropping by about 0.5% in 90° rim angle for a glass enveloped receiver. The magnitudes of LCR, η_{opt} and C_{avg} were estimated to drop almost linearly with an increase in mirror focal length.

A defocus dislocation of the receiver improves the uniformity of the LCR distribution on the bottom half of the receiver. Off-focus dislocation of the receiver, and inward deviation of the mirror profile from its ideal shape increase the C_{max} and non-uniformity of the LCR distribition. On the other hand, out-focus dislocation of the receiver and solar tracking error break the bi-symmetry of the normal LCR profile. Off-focus and defocus dislocation of the receiver more than about 0.75r (r is radius of the receiver), out-focus dislocation more than about 0.15r, deviation of the mirror profile more than 0.375°, and tracking error more than 0.6° were observed to cause rapid decrease of the optical efficiency and the average light concentration of the collector.

Acknowledgments: This article is a part of a PhD project that is supported by a QUT post graduate research award and by a CSIRO Flagship collaboration fund PhD top-up scholarship through the Energy Transformed Flagship.

Author Contributions: This article is produced from the PhD work of Majedul Islam. Majedul Islam conceived, designed and accomplished the research, and drafted the article under the principle supervision of Azharul Karim, who is the leader of the research team. Prasad Yarlagadda and Sarah Miller were the associate supervisors for the PhD program. Azharul Karim extremely motivated Majedul Islam to prepare the article. Azharul Karim also reviewed and edited the article. Sarah Miller accomplished a proofread for the article.

Conflicts of Interest: No known conflicts of interest could be disclosed.

Nomenclature

C	Concentration or Constant
CF	Concentration Falling zone of a normal LCR profile under ideal condition
CI	Concentration Increasing zone of a normal LCR profile under ideal condition
DS	Direct Sun zone of a normal LCR profile under ideal condition
d	Depth, diameter, deviation, dislocation
D	Direction vector
DNI	Direct Normal Irradiance
E	Error
f	Focal length
GC	Geometric Concentration (×) (Ratio of mirror aperture area to receiver surface area)
GT	Glass Tube
$I(\varphi)$	Sunshape or light intensity as a function of deflection angle
LCR	Local Concentration Ratio (sun)
LS2	Luz Solar 2 collector
MAD	Mean Absolute Deviation
MC	Monte Carlo
MCRT	Monte Carlo Ray Tracing
N	Normal vectors, Number of rays per unit aperture area of the sunshape
n	Refractive indices of glass and air
P	Point of light incidence
PT	Parabolic Trough
PTC	Parabolic Trough Concentrator
r	Radius of the receiver
RT	Receiver Tube
RS	Receiver Shadowing zone of a normal LCR profile under ideal condition
sun	Unit of light concentration (1 kW/m^2)
t	Thickness
TC	Test Conditions
W	Half width of the mirror
V	Variable or varied
X, Y, Z	Cartesian coordinate system
X, r, β	Polar coordinate system
Symbols	
η_{opt}	Optical efficiency
β	Angular location on the receiver
ψ	Rim angle (°) of the mirror
φ	Deflection angle of sun
Û, Ŭ	Inward and outward angular deviation of the mirror profile (°)
τ_{GT}	Transmittance of glass tube
ϱ_{PT}	Reflectance of mirror
↑, ↓	Increase or upward, decrease or downward
→↔←|	lateral direction
Suffixes	
abs	Absolute
avg	Average
Expt	Experimental or measured value
max	Maximum
min	Minimum
o	Outer or outside

References

1. Karim, M.A.; Perez, E.; Amin, Z.M. Mathematical modelling of counter flow v-grove solar air collector. *Renew. Energy* **2014**, *67*, 192–201. [CrossRef]
2. Thomas, A.; Guven, H.M. Effect of optical errors on flux distribution around the absorber tube of a parabolic trough concentrator. *Energy Convers. Manag.* **1994**, *35*, 575–582. [CrossRef]
3. Pottler, K.; Lupfert, E.; Johnston, G.H.G.; Shortis, M.R. Photogrammetry: A powerful tool for geometric analysis of solar concentrators and their components. *J. Sol. Energy Eng.* **2005**, *127*, 94–101. [CrossRef]
4. Shortis, M.; Johnston, G. Photogrammetry: An available surface characterization tool for solar concentrators, part II: Assessment of surfaces. *J. Sol. Energy Eng.* **1997**, *119*, 286–291. [CrossRef]
5. Shortis, M.R.; Johnston, G.H.G. Photogrammetry: An available surface characterization tool for solar concentrators, part I: Measurements of surfaces. *J. Sol. Energy Eng.* **1996**, *118*, 146–150. [CrossRef]
6. Riffelmann, K.-J.; Neumann, A.; Ulmer, S. Performance enhancement of parabolic trough collectors by solar flux measurement in the focal region. *Sol. Energy* **2006**, *80*, 1303–1313. [CrossRef]
7. Schiricke, B.; Pitz-Paal, R.; Lupfert, E.; Pottler, K.; Pfander, M.; Riffelmann, K.-J.; Neumann, A. Experimental verification of optical modeling of parabolic trough collectors by flux measurement. *J. Sol. Energy Eng.* **2009**, *131*, 11004–11006. [CrossRef]
8. Jeter, S.M. Analytical determination of the optical performance of practical parabolic trough collectors from design data. *Sol. Energy* **1987**, *39*, 11–21. [CrossRef]
9. Jeter, S.M. Calculation of the concentrated flux density distribution in parabolic trough collectors by a semifinite formulation. *Sol. Energy* **1986**, *37*, 335–345. [CrossRef]
10. Jeter, S.M. The distribution of concentrated solar radiation in paraboloidal collectors. *J. Sol. Energy Eng.* **1986**, *108*, 219–225. [CrossRef]
11. Daly, J.C. Solar concentrator flux distributions using backward ray tracing. *Appl. Opt.* **1979**, *18*, 2696–2699. [CrossRef] [PubMed]
12. Riveros, H.G.; Oliva, A.I. Graphical analysis of sun concentrating collectors. *Sol. Energy* **1986**, *36*, 313–322. [CrossRef]
13. Riveros-Rosas, D.; Sanchez-Gonzalez, M.; Estrada, C.A. Three-dimensional analysis of a concentrated solar flux. *J. Sol. Energy Eng.* **2008**, *130*, 14503–14504. [CrossRef]
14. Cheng, Z.D.; He, Y.L.; Xiao, J.; Tao, Y.B.; Xu, R.J. Three-dimensional numerical study of heat transfer characteristics in the receiver tube of parabolic trough solar collector. *Int. Commun. Heat Mass Transf.* **2010**, *37*, 782–787. [CrossRef]
15. He, Y.-L.; Xiao, J.; Cheng, Z.-D.; Tao, Y.-B. A MCRT and FVM coupled simulation method for energy conversion process in parabolic trough solar collector. *Renew. Energy* **2011**, *36*, 976–985. [CrossRef]
16. Cheng, Z.D.; He, Y.L.; Cui, F.Q. A new modelling method and unified code with mcrt for concentrating solar collectors and its applications. *Appl. Energy* **2013**, *101*, 686–698. [CrossRef]
17. Grena, R. Optical simulation of a parabolic solar trough collector. *Int. J. Sustain. Energy* **2009**, *29*, 19–36. [CrossRef]
18. Wirz, M.; Roesle, M.; Steinfeld, A. Three-dimensional optical and thermal numerical model of solar tubular receivers in parabolic trough concentrators. *J. Sol. Energy Eng.* **2012**, *134*, 041012. [CrossRef]
19. Yang, B.; Zhao, J.; Xu, T.; Zhu, Q. Calculation of the concentrated flux density distribution in parabolic trough solar concentrators by monte carlo ray-trace method. In Proceedings of the 2010 Symposium on Photonics and Optoelectronics, Chengdu, China, 19–21 June 2010.
20. Kalogirou, S.A.; Lloyd, S.; Ward, J.; Eleftheriou, P. Design and performance characteristics of a parabolic-trough solar-collector system. *Appl. Energy* **1994**, *47*, 341–354. [CrossRef]
21. Coventry, J.S. Performance of a concentrating photovoltaic/thermal solar collector. *Sol. Energy* **2005**, *78*, 211–222. [CrossRef]
22. Kabakov, V.I.; Levin, L.B. A choice of the position of receiver with photocells in parabolic trough concentrator. *Sol. Energy Mater. Sol. Cells* **1994**, *33*, 45–49. [CrossRef]
23. Islam, M.; Karim, M.A.; Saha, S.C.; Miller, S.; Yarlagadda, P.K.D.V. Development of empirical equations for irradiance profile of a standard parabolic trough collector using monte carlo ray tracing technique. *Adv. Mater. Res. Energy Dev.* **2014**, *860–863*, 180–190. [CrossRef]

24. Dudley, V.E.; Kolb, G.J.; Mahoney, A.R.; Mancini, T.R.; Matthews, C.W.; Sloan, M.; Kearney, D. *Test Results: SEGS LS-2 Solar Collector*; National Technical Information Service, US Department of Commerce: Springfield, VA, USA, 1994; p. 139.
25. Buie, D.; Dey, C.J.; Bosi, S. The effective size of the solar cone for solar concentrating systems. *Sol. Energy* **2003**, *74*, 417–427. [CrossRef]
26. Forristall, R. *Heat Transfer Analysis and Modeling of a Parabolic Trough Solar Receiver Implemented in Engineering Equation Solver*; Technical Report No. NERL/TP-550-34169; National Renewable Energy Laboratory: Golden, CO, USA, 2003.